Changes in the intermediate water mass formation rates in the global ocean for the Last Glacial Maximum, mid-Holocene and pre-industrial climates

I. Wainer,[1] M. Goes,[2] L. N. Murphy,[3,4] and E. Brady[5]

Received 26 January 2012; revised 29 May 2012; accepted 19 July 2012; published 28 August 2012.

[1] The paleoclimate version of the National Center for Atmospheric Research Community Climate System Model version 3 (NCAR-CCSM3) is used to analyze changes in the water formation rates in the Atlantic, Pacific, and Indian Oceans for the Last Glacial Maximum (LGM), mid-Holocene (MH) and pre-industrial (PI) control climate. During the MH, CCSM3 exhibits a north-south asymmetric response of intermediate water subduction changes in the Atlantic Ocean, with a reduction of 2 Sv in the North Atlantic and an increase of 2 Sv in the South Atlantic relative to PI. During the LGM, there is increased formation of intermediate water and a more stagnant deep ocean in the North Pacific. The production of North Atlantic Deep Water (NADW) is significantly weakened. The NADW is replaced in large extent by enhanced Antarctic Intermediate Water (AAIW), Glacial North Atlantic Intermediate Water (GNAIW), and also by an intensified of Antarctic Bottom Water (AABW), with the latter being a response to the enhanced salinity and ice formation around Antarctica. Most of the LGM intermediate/mode water is formed at $27.4 < \sigma_\theta < 29.0$ kg/m^3, while for the MH and PI most of the subduction transport occurs at $26.5 < \sigma_\theta < 27.4$ kg/m^3. The simulated LGM Southern Hemisphere winds are more intense by 0.2–0.4 dyne/cm^2. Consequently, increased Ekman transport drives the production of intermediate water (low salinity) at a larger rate and at higher densities when compared to the other climatic periods.

Citation: Wainer, I., M. Goes, L. N. Murphy, and E. Brady (2012), Changes in the intermediate water mass formation rates in the global ocean for the Last Glacial Maximum, mid-Holocene and pre-industrial climates, *Paleoceanography*, *27*, PA3101, doi:10.1029/2012PA002290.

1. Introduction

[2] Ventilation in the Southern and Arctic oceans contributes to significant uptake of heat and atmospheric gases. In this respect, the intermediate waters are recognized to have a major impact on the oceanic sink for anthropogenic CO_2 [e.g., *Sabine et al.*, 2004; *Sabine and Tanhua*, 2010], but also to contain the largest uncertainties in carbon inventories [e.g., *McNeil et al.*, 2003]. The role of the formation of intermediate waters, in particular the Antarctic Intermediate Water (AAIW), and their ability to redistribute heat and freshwater within the upper ocean has been the subject of many studies [*Pahnke and Zahn*, 2005; *Sloyan and Rintoul*, 2001; *Sørensen et al.*, 2001; *Sloyan and Kamenkovich*, 2007].

[3] The AAIW is a low salinity water mass that is formed in the South Atlantic and South Pacific oceans [*Taft*, 1963], and transported northward into the Indian, Pacific and Atlantic along subtropical gyres. AAIW fills most of the Southern Hemisphere, and parts of the North Pacific and North Atlantic Oceans at about 800 to 1200 m depth or within $\sigma_\theta = 26.9 - 27.5$ kg/m^3 isopycnals [*Talley*, 1996]. AAIW has been defined as the densest class of the Subantarctic Mode Water (SAMW) [*McCartney*, 1977], with which it shares similar dynamics [*Drijfhout et al.*, 2005]. In the formation region, AAIW (and SAMW) is characterized by a thick (low potential vorticity) outcropping mixed layer just north of the Subantarctic Front (SAF), with formation associated with the winter properties of the mixed layer and winds [*Karstensen and Quadfasel*, 2002].

[4] In the South Pacific, the intermediate waters that spread northward from the Southern ocean are also denominated the Pacific Intermediate Water (PIW) [*Talley*, 1999]. The North Pacific is currently the only place in the Northern Hemisphere that forms waters at intermediate depths, the North

[1]Departamento de Oceanografia Física, Universidade de São Paulo, São Paulo, Brazil.
[2]CIMAS, University of Miami, and NOAA/AOML, Miami, Florida, USA.
[3]Lawrence Berkeley National Laboratory, Berkeley, California, USA.
[4]Now at Rosenstiel School of Marine and Atmospheric Science, University of Miami/RSMAS, Miami, Florida, USA.
[5]National Center for Atmospheric Research, Boulder, Colorado, USA.

Corresponding author: I. Wainer, Departamento de Oceanografia Física, Universidade de São Paulo, Praça do Oceanográfico 191, Cidade Universitária, São Paulo, SP 05508120, Brazil. (wainer@usp.br)

0883-8305/12/2012PA002290

Pacific Intermediate Water (NPIW), which is formed between σ_θ = 26.2 − 26.9 kg/m^3 and is found generally north of 15°N, at depths of 300 to 800 m [*Talley*, 1993].

[5] Underneath the intermediate waters are the deep waters. The North Atlantic Deep Water (NADW) formation occurs at a high rate in the North Atlantic through convection in the Arctic ocean, which makes the Atlantic high ventilated in these depths. In the North Pacific the present abyssal circulation flows from the south, upwells to mid-depth and returns south as the Pacific Deep Water (PDW) below the NPIW [*Schmitz*, 1996]. Below 4000 m, the cold and fresh Antarctic Bottom Water (AABW) occupies the ocean across the globe.

[6] Previous modeling and observational paleoclimate studies [*Adkins et al.*, 2002; *Pahnke et al.*, 2008, and references therein] have shown that the structure of the water masses we know today has experienced considerable changes. For instance, proxy reconstructions of the Last Glacial Maximum (LGM) [*Adkins et al.*, 2002] show that the deep oceans were more homogeneous, with stronger influence from the southern waters, which were much saltier than they are today. The North Atlantic was much fresher, and the NADW formation was suppressed, giving rise to a fresh north Atlantic intermediate formation (GNAIW). In the North Pacific, proxy data ($\Delta^{14}C$) suggest a more vigorous and expanded NPIW within the 1500–2000 m water column during the LGM, with a smaller exchange from deep to intermediate waters [*Toggweiler*, 1999; *Matsumoto et al.*, 2002]. This process would be responsible for increasing deep carbon reservoirs in the deep Pacific Ocean during the LGM [*Herguera et al.*, 2010]. The storing and release of heat, carbon and other ocean tracers can contribute significantly, and potentially trigger changes in the earth's climate system [*Cléroux et al.*, 2011; *Skinner et al.*, 2010]. Changes in water properties are in part a consequence of subduction, and wind and mixing driven processes, as well as changes in the ocean interior that occur after subduction [*Wong et al.*, 1999; *Joyce et al.*, 1998].

[7] In this study, we quantify the rate of water formation across the base of the mixed layer for past climates. We analyze simulation results for the LGM (approximately 21,000 years before present), the mid-Holocene (MH, approximately 6,000 years before present) and the pre-industrial control (PI). These simulations are performed with the National Center for Atmospheric Research (NCAR) Community Climate System Model version 3 (CCSM3), which are described in detail in *Otto-Bliesner et al.* [2006]. Our main motivation is to understand the response of the global subduction rates to the integrated changes during past climates, such as the hydrological cycle, ocean temperature conditions, greenhouse gases concentrations and orbital forcing, and their link to the related changes in the water mass properties. Previous modeling studies analyzed these paleo climates in terms of 3-dimensional circulation [*Clauzet et al.*, 2007; *Otto-Bliesner et al.*, 2007], NADW and AABW water mass formation [e.g., *Shin et al.*, 2003b; *Liu et al.*, 2005], and tropical variability [e.g., *Liu et al.*, 2000; *Braconnot et al.*, 2007b; *Otto-Bliesner et al.*, 2009]. We improve the current knowledge by focusing on the AAIW formation and changes in intermediate depths, and determine plausible mechanisms for such changes. This paper is organized as follows. Section 2 describes the model and model experiments. Section 3 describes the general water mass features in the model simulations and their subduction properties. Section 4 includes discussions of the results and conclusions.

2. Model Description

[8] The CCSM3 is a coupled climate general circulation model consisting of four main components, the atmosphere, ocean, sea ice and land. The atmospheric model is the NCAR Community Atmosphere Model version 3 (CAM3), a three-dimensional primitive equation model solved with the spectral method in the horizontal [*Collins et al.*, 2006]. The ocean model is the NCAR implementation of the Parallel Ocean Program (POP), a three-dimensional primitive equation model in spherical polar coordinates with a dipole grid and a 40 level vertical z coordinate [*Gent et al.*, 2006]. Poles are located in Greenland and Antarctica.

[9] The sea ice model is a dynamic–thermodynamic model, which includes a subgrid-scale ice thickness parameterization and elastic–viscous–plastic rheology [*Briegleb et al.*, 2004]. It includes sea ice dynamics and exchanges of salt between sea ice and the surrounding ocean. The land model includes a river routing scheme and specified land cover and plant functional types [*Dickinson et al.*, 2006]. The atmosphere and land components share a horizontal resolution of T42, approximately 2.8° in latitude and longitude. The ocean and sea ice components share a horizontal resolution that is approximately 1° in latitude and longitude with higher resolution in the Tropics and North Atlantic.

[10] Concentrations of the atmospheric greenhouse gases in the CCSM3 paleo simulations are adjusted based on ice core measurements [*Flückiger et al.*, 1999; *Dällenbach et al.*, 2000; *Monnin et al.*, 2001] and follow the protocols established by PMIP2 [*Braconnot et al.*, 2007a]. Their overall effect are a reduction in radiative forcing of −2.76 W m^{-2} for the LGM and only −0.07 W m^{-2} for the mid-Holocene, with the latter only due to a reduction in methane concentration. In addition to reduced atmospheric greenhouse gases, other major differences are the changes in the earth's orbital parameters, the presence of ice sheets, and exposed coastline and shallow sills due to sea level lowering. In the LGM, elevation and ice sheet extent are taken from the ICE-5G reconstruction [*Peltier*, 2004]. Major changes include increased elevation and ice extent over Antarctica, the Southern Andes and throughout much of the high latitude Northern Hemisphere, with the exception of central Greenland. MH uses the same topography and ice elevation data as PI. The solar constant is set to 1365 W m^{-2} in all three simulations. The model components are integrated separately to obtain an appropriate initial state of the coupled system prior to full coupling. The numerical simulations of the MH and LGM (except for the ocean) are initialized from the PI run. The LGM ocean is initialized with a previous LGM simulation *Shin et al.* [2003a]. Both are run for 300 years. At this time, as discussed in *Otto-Bliesner et al.* [2006], the simulations reach quasi-equilibrium, with small trends present, particularly at Southern Hemisphere high latitudes and the deep ocean. The mean climate results analyzed are averages for the last 150 years of the LGM and MH runs. A detailed description of the paleoclimate model and experiments are

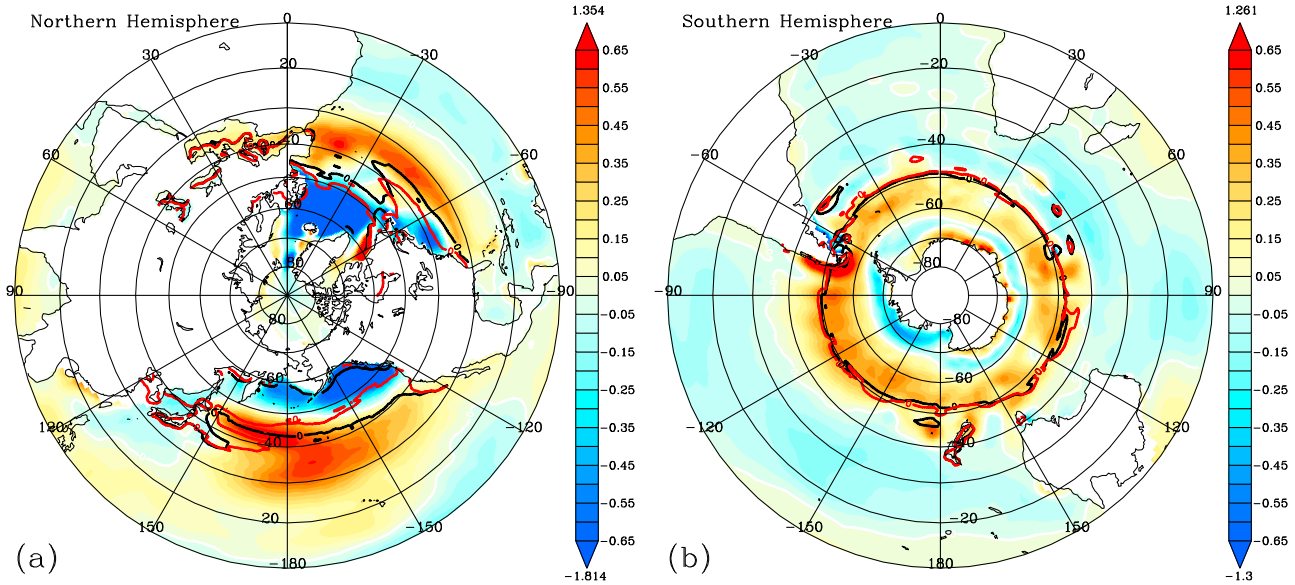

Figure 1. Difference field (LGM - PI) for (a) Northern and (b) Southern Hemisphere Zonal wind stress (NHZW and SHZW, respectively) in dyne/cm^2. Also shown are the positions of zero wind stress curl for the LGM (black contours) and PI (red contours). The LGM winds are more intense by 0.2–0.4 (dyne/cm^2) in the south.

discussed in *Otto-Bliesner et al.* [2006] and *Clauzet et al.* [2007].

3. Results

3.1. General Features

[11] Changes in the annual surface ocean response during the LGM and MH glacial periods in comparison to the present-day have been extensively discussed in previous modeling studies [e.g., *Liu et al.*, 2000, 2003; *Shin et al.*, 2003a, 2003b; *Otto-Bliesner et al.*, 2006, 2007; *Clauzet et al.*, 2007, 2008; *Otto-Bliesner et al.*, 2009]. Here, for the sake of completeness, we summarize the general hydrography and and atmospheric fluxes in CCSM3.

[12] The spatial changes in the intensity of the time-averaged zonal wind stress is shown in Figure 1. In the Southern Hemisphere, there is a strengthening of the westerlies (positive anomalies) in the LGM. Because of the complex topography, LGM winds are more intense on the Pacific side of the South American coast and weaker on the Atlantic side. Between 40°S and the equator, wind changes are smaller. In the Northern Hemisphere there is a shift of the zero wind stress curl southward in the LGM, but no visible shift is seen in the Southern Hemisphere, consistent with *Shin et al.* [2003a].

[13] The mean zonal wind anomalies for the MH (not shown) are an order of magnitude smaller that the ones in the LGM. Previous studies [e.g., *Liu et al.*, 2003] show substantial changes of the seasonal wind stress during the MH, but small changes in the annual mean because seasonal wind anomalies tend to be opposite in winter and summer in response to the anomalous insolation forcing.

[14] The CCSM3 LGM global annual sea surface temperature (SST) is on average 4.5°C cooler relative to PI conditions [*Otto-Bliesner et al.*, 2006], which is stronger than ocean cooling of 2°C in previous LGM simulations [*Shin et al.*, 2003a, 2003b] and SST proxy reconstruction (CLIMAP, 1981). The ocean surface is colder and saltier in most of the places (Figure 2), caused by a weaker hydrological cycle due to a colder climate. High sea surface salinity (SSS) anomalies of ≈7 psu are observed in the North Atlantic, and the highest temperature anomalies are found in the North Pacific and North Atlantic, which is related not only with brine rejection due to more ice formation, but with the migration of the subtropical gyres southward (Figure 2). Warming in the Bering Sea and Gulf of Alaska are related to changes in the upper level dynamics and a deepened Aleutian low, which advects warm air poleward into the Gulf of Alaska [*Otto-Bliesner et al.*, 2006].

[15] A comparison of the LGM simulation used here with proxy data from the South Atlantic Ocean has been previously performed by *Clauzet et al.* [2008], which shows some regional discrepancies. The largest biases occur in the eastern, equatorial and in the high latitudes of the basin, while a good agreement between the model and reconstructed data is reached in the western and central parts of the South Atlantic.

[16] The annual mean surface temperature and salinity anomalies in the MH relative to PI are less substantial than in the LGM (Figures 2b and 2d). Overall, there is a symmetric response that reveals a tropical cooling and high latitude warming. This feature agrees with the differences shown in Figure 2 and is consistent with a synthesis of mid-Holocene paleo-SST records [*Liu et al.*, 2003]. Previous studies [*Otto-Bliesner et al.*, 2006] show that Increased boreal summer insolation reduces Northern Hemisphere sea-ice, which enhances the warming due to the ice-albedo feedback. Melting of sea-ice leads to a freshening of the northern high latitudes, as observed in Figure 2b. High positive salinity anomalies located in the North Pacific (≈0.8 psu) and

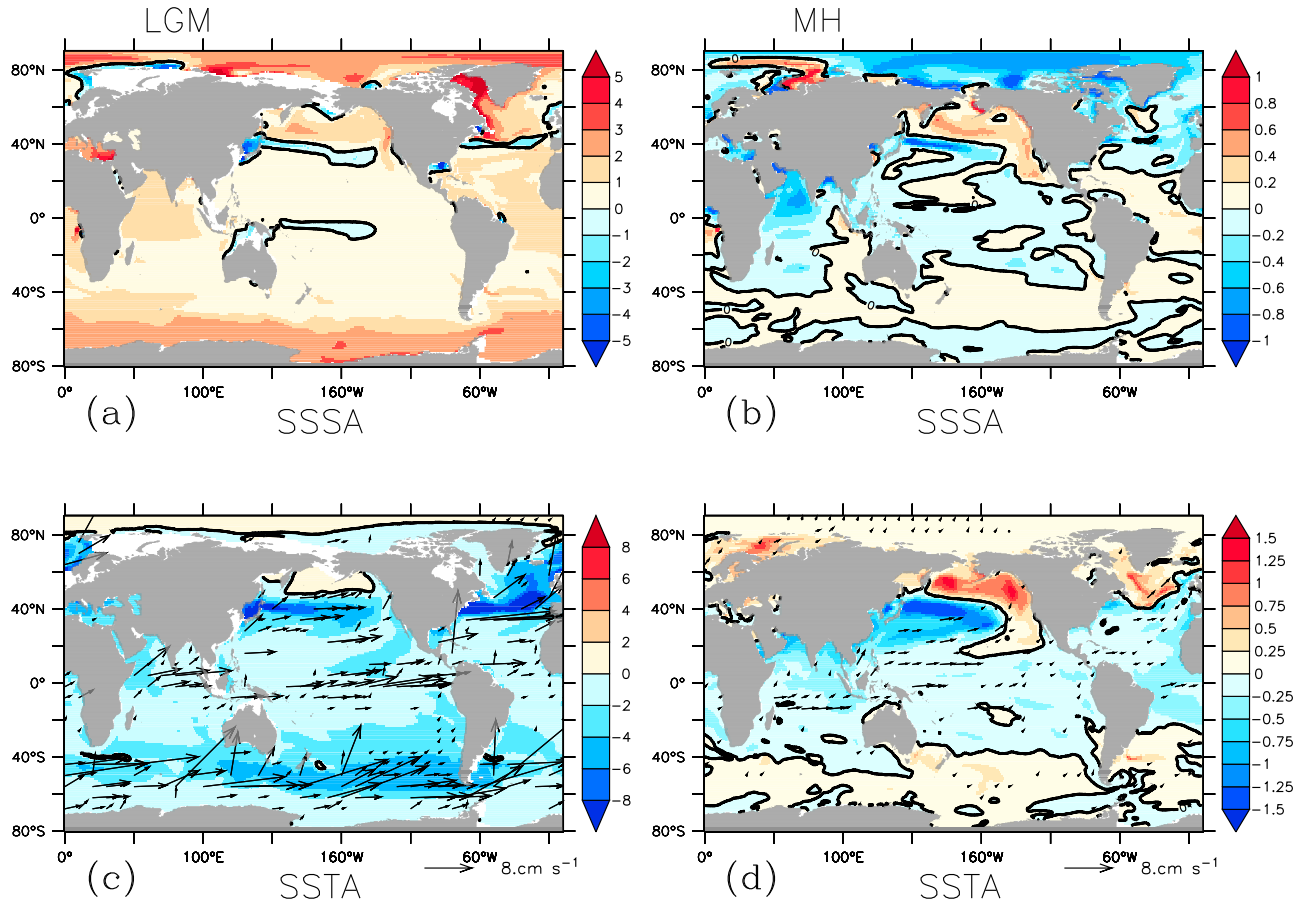

Figure 2. Global annual sea surface salinity (SSSA) and temperature (SSTA) differences relative to PI for the (a, c) LGM and (b, d) MH. Average annual velocity differences in the upper 80 m of the ocean are overlaid on the temperature panels for the respective periods. Only velocity differences about 1 cm/s are displayed.

Tropical Atlantic (≈0.2 psu) are due to atmospheric drying *Braconnot et al.* [2007a].

[17] These surface differences from the paleo simulations against the PI reflect changes in the whole water column. Regarding the PI, zonally averaged sections of temperature an salinity with depth (Figures 3 and 4, upper panels) show that the North Atlantic is characterized by strong formation of relatively cold (about 2 to 4°C; Figure 3a) and salty (about 35 psu; Figure 4a) NADW at about 3000 m. In the South Atlantic, the low salinity AAIW tongue is observed at about 1000 m, mostly south of the equator (Figure 3a). The formation region of the AAIW (at about 50°S) is characterized by a salinity minimum between the σ_θ = 26.5 − 27 kg/m^3 isopycnals. In the Indo-Pacific, deep waters (below 1500 m) are generally colder (≈0–2°C; Figure 3b) and fresher (≈34.6 psu; Figure 4b) than the Atlantic conterpart, and low salinity intermediate waters (PIW and NPIW) fill most of the basin between 1000–2000 m (Figure 4b). An excess of precipitation over evaporation results in lower salinity values over the North Pacific. As a result the North Pacific shows a stronger stratification and shallower mixed layer, favoring formation of lower density waters with respect to the North Atlantic.

[18] Significant differences are manifested in the hydrographic fields of the LGM (Figures 3c, 3d, 4c, and 4d). In the North Atlantic, the deep signature of the NADW is not observed during the LGM (Figure 4c). Instead, stronger formation of southern bottom waters advect strong salinity anomalies >1.5 psu below 1500 m (Figure 3c), confining the northern water formation to the upper 1500–2000 m of the water column. North Atlantic water formation is more than 4°C colder than the PI, but relatively fresher in comparison to the AABW in the LGM, therefore forming a tongue of Glacial North Atlantic Intermediate Water (GNAIW). In the Southern Ocean, the LGM features a much denser and wider Antarctic Bottom Water (AABW) (Figures 4c and 4d), in agreement with proxy observations [*Adkins et al.*, 2002; *Marchitto and Broecker*, 2006], indicating a stronger AABW formation. The Southern Ocean, which is the source region for the AABW, contains higher surface salinity and lower temperature (Figure 4a and 4b) in the LGM. These surface characteristics have been associated with an enhanced, colder and saltier AABW due to intensified ice formation around Antarctica [*Shin et al.*, 2003a; *Liu*, 2006].

[19] In the South Indo-Pacific, as observed in the South Atlantic during the LGM, formation of AABW and Pacific Deep Water (PDW) are increased (Figure 4d). The volume increase of the PDW displaces the LGM intermediate waters in the Indo-Pacific to shallower depths (above 800 m). The

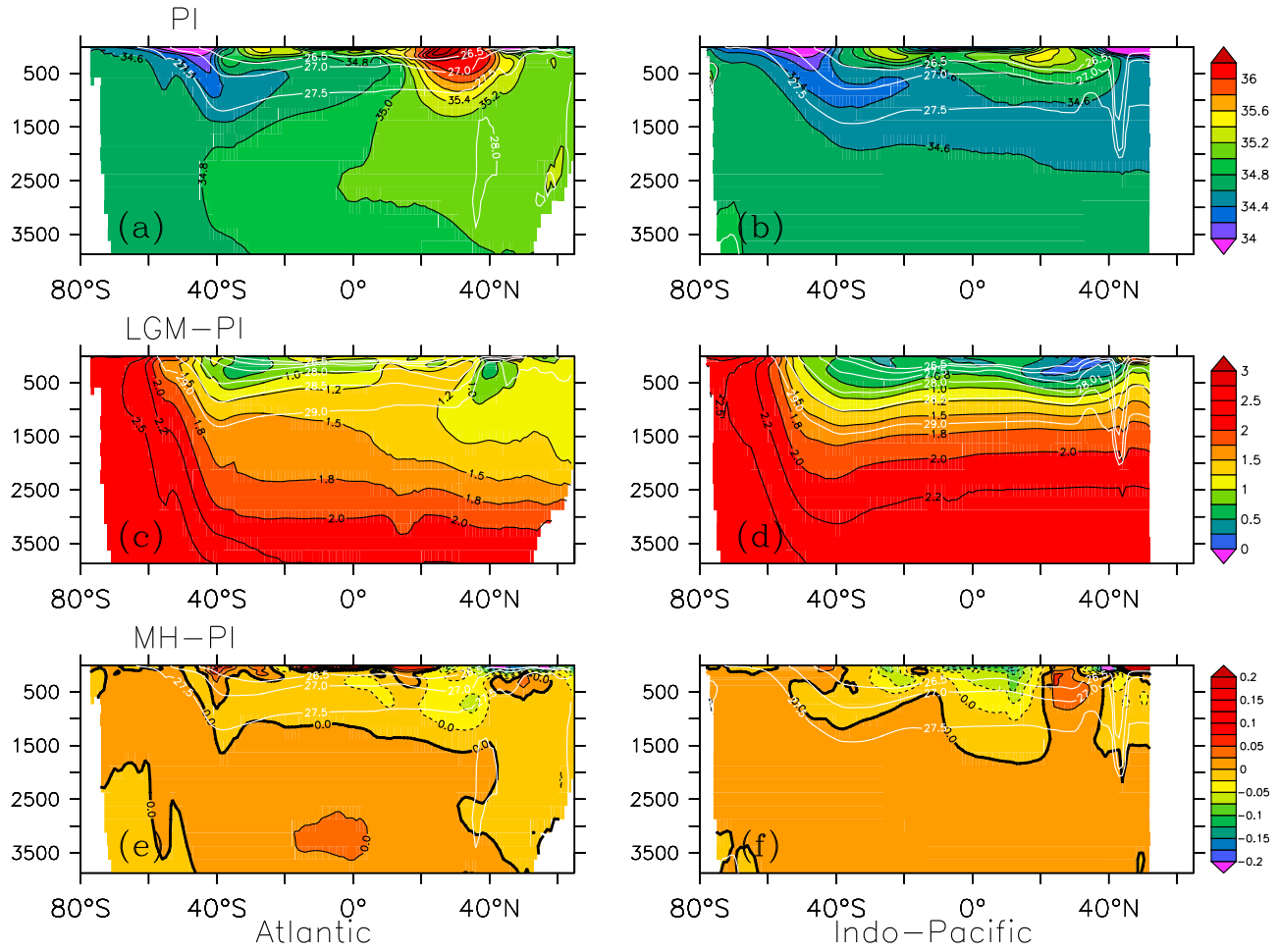

Figure 3. Zonal average salinity (psu) for the PI in the (a) Atlantic and (b) Indo-Pacific basins. Salinity differences relative to PI for the (c, d) LGM and (e, f) MH, with the respective PI panel positions for the Atlantic (left) and Indo-Pacific (right) basins. Zonal average potential density contours (kg m^{-3}) are overlaid in white for each basin and geological period.

intermediate waters suffer the highest temperature anomalies in the Indo-Pacific, up to −3.5°.

[20] The density contours in Figures 3c, 3d, 4c, and 4d suggest a higher stratification in the upper 1500 m during the LGM, and a more homogeneously cold and stagnant deep layer in the Pacific (4d). For instance, the σ_θ = 29 kg/m^3 density level is around 1000–1500 m depth in the LGM (Figures 4c and 4d), at about the same depth of the σ_θ = 27.5 kg/m^3 density level in the PI and MH (Figures 4a, 4b, 4e, and 4f).

[21] The hydrographic differences of the MH relative to PI are mostly restricted to the upper 1500 m (Figure 3e and 3f). Changes in the MH are largely due to anomalous seasonal insolation [*Liu et al.*, 2003]. In agreement with [*Liu et al.*, 2003], the Pacific ocean changes in the MH are characterized by a cooling and freshening in the Northern Hemisphere and a warming in the Southern Hemisphere (Figure 3f). However, the Atlantic ocean shows warming in the high northern latitudes, related to sea-ice reduction and resulting ice-albedo feedback. As oppose to the upper layers, below 1500 m the MH is in general slightly saltier (order of 10^{-3} psu) and warmer (order of 10^{-2}°C).

[22] The density range of each water mass can be retrieved with a good approximation by their θ-S properties. Here we use θ-S diagrams to select the σ_θ ranges of the main water masses for the different geological periods in the Pacific, Indian, and Atlantic basins (Figure 5). The potential temperature and salinity fields are first interpolated onto potential density surfaces, similarly to *Downes et al.* [2010], and then averaged over each basin between 15–60 degrees of latitude. Previous model studies have already shown θ-S relationships for the LGM and MH [e.g., *Shin et al.*, 2003a; *Liu et al.*, 2005; *Otto-Bliesner et al.*, 2006], and their comparison to the θ-S obtained from proxy data [*Adkins et al.*, 2002] suggests reasonable agreement with observations.

[23] During the PI an MH, the salinity minimum of approximately 34.2 representing the AAIW core is observed at about σ_θ = 27.2 kg/m^3 in the South Atlantic and South Pacific (5c, d). Considering the SAMW and AAIW together, their range spans from σ_θ = 26.4 − 27.4 kg/m^3. In the South Atlantic (Figure 5c), the MH shows a clear upward displacement in the mean θ-S, and therefore a small warming (on the order of 0.03°C) in the deep layers relative to the isopycnals.

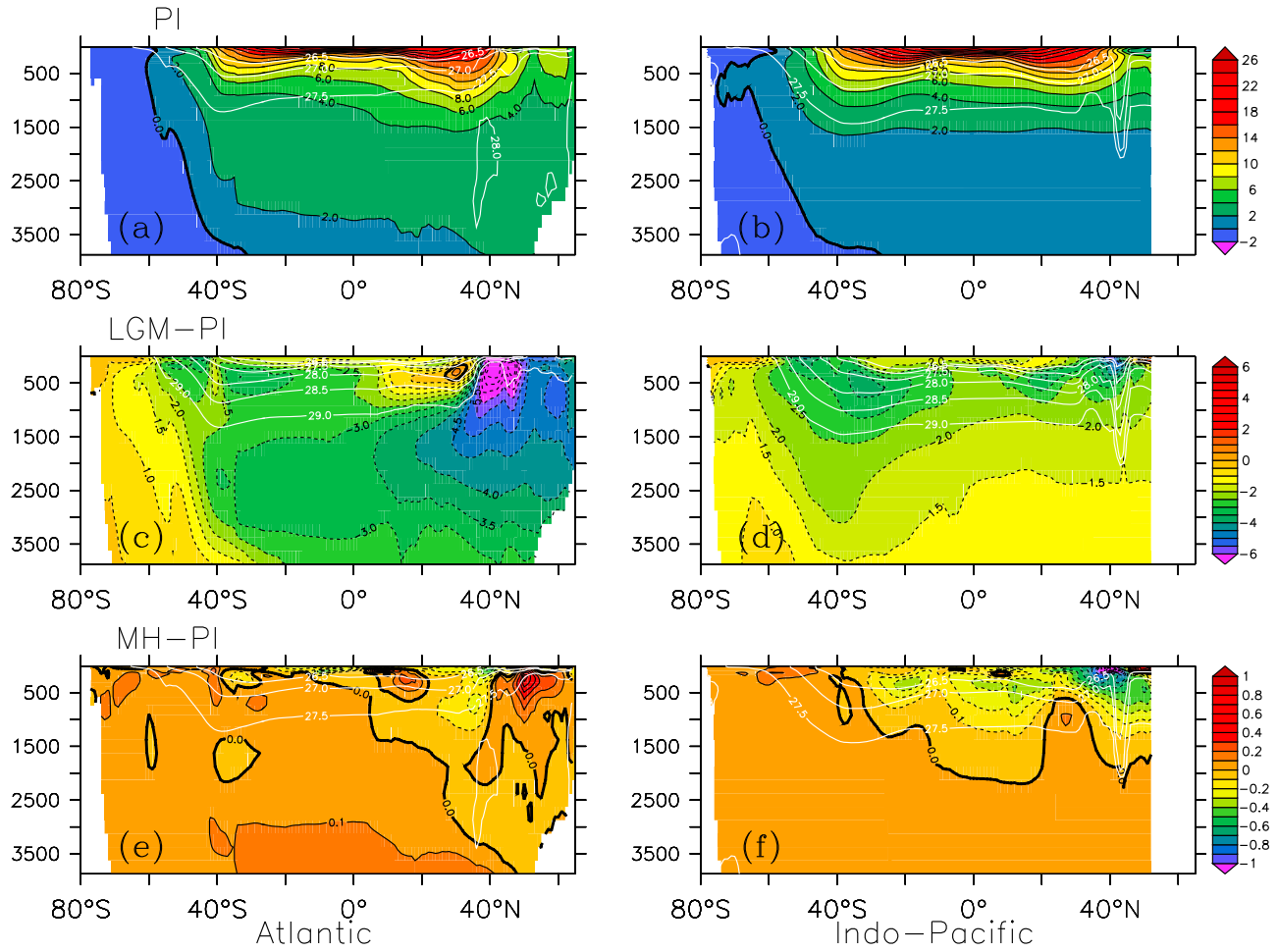

Figure 4. Same as Figure 3 but for potential temperature (°C).

[24] In the LGM the AAIW salinity minimum is denser, centered at about $\sigma_\theta = 28.0$ kg/m^3 (Figure 5c and 5d), and with broader AAIW + SAMW range of $\sigma_\theta = 27.4 - 29.0$ kg/m^3. Below $\sigma_\theta = 28.0$ there is an almost linear increase in salinity and accompanying decrease in temperature all the way to the bottom in the Pacific and South Atlantic. This behavior is consistent with the extension of the PDW in the Pacific and AABW in the Pacific and Atlantic, which is a feature attributed to the ocean during the LGM [e.g., *Clauzet et al.*, 2007; *Fischer et al.*, 2010; *Oppo and Fairbanks*, 1987].

[25] In the North Pacific (Figure 5b), the NPIW minimum in the MH (34.5) is larger than in the PI (34.3), but in both periods the minimum is located at about $\sigma_\theta = 26.4$ kg/m^3, with total range of 25.7–26.8 kg/m^3. Between PI and MH the differences in deeper waters are negligible. In the LGM, the glacial NPIW minimum of 34.8 is centered at $\sigma_\theta = 27.0$ kg/m^3, ranging form $\sigma_\theta = 26.5 - 27.5$ kg/m^3. The North Atlantic features the NADW with salinity of 35 psu (Figure 5a) in the PI and MH, and expands through a large part of the density parameter space. The GNAIW, which replaces the NADW in the LGM, shows a minimum salinity of 36.3, and ranges from $\sigma_\theta = 28.5 - 29.4$ kg/m^3.

3.2. Subduction Rates Calculations

[26] The amount of water mass formation that departs the mixed layer downward across the permanent pycnocline is measured by the annual subduction rate [*Cushman-Roisin*, 1987]. In the absence of interannual or shorter variability of the mixed layer, the fluid leaving the mixed layer during the winter/spring time can irreversibly enter the permanent thermocline [*Stommel*, 1979]. Here we use the same formulation of *Goes et al.* [2008] to diagnose the annual subduction across the base of the ocean mixed layer as a function of potential density at the region of the thermocline outcropping. According to *Goes et al.* [2008] formulation, the annual subduction rate is calculated with respect to the maximum annual mixed layer depth (H). The volume transfer of water subducted for each basin as a function of density is obtained by integrating the positive values (downward) of the Eulerian subduction rate, which is defined at each grid point, over the surface bounded by two adjacent isopycnals along H. This calculation is performed as follows:

$$Sub(\sigma_\theta) = -\oint_{\sigma_\theta - \frac{\Delta\sigma_\theta}{2}}^{\sigma_\theta + \frac{\Delta\sigma_\theta}{2}} \left[\mathbf{u}_H \cdot \nabla H + w_H\right] dA, \qquad (1)$$

where the first term on right hand side of (1) represents the lateral induction across a sloping mixed layer base and the second term accounts for the vertical entrainment. In Equation (1), $\mathbf{u}_H$ and w_H are the annual average of horizontal and vertical velocities, respectively, linearly interpolated to

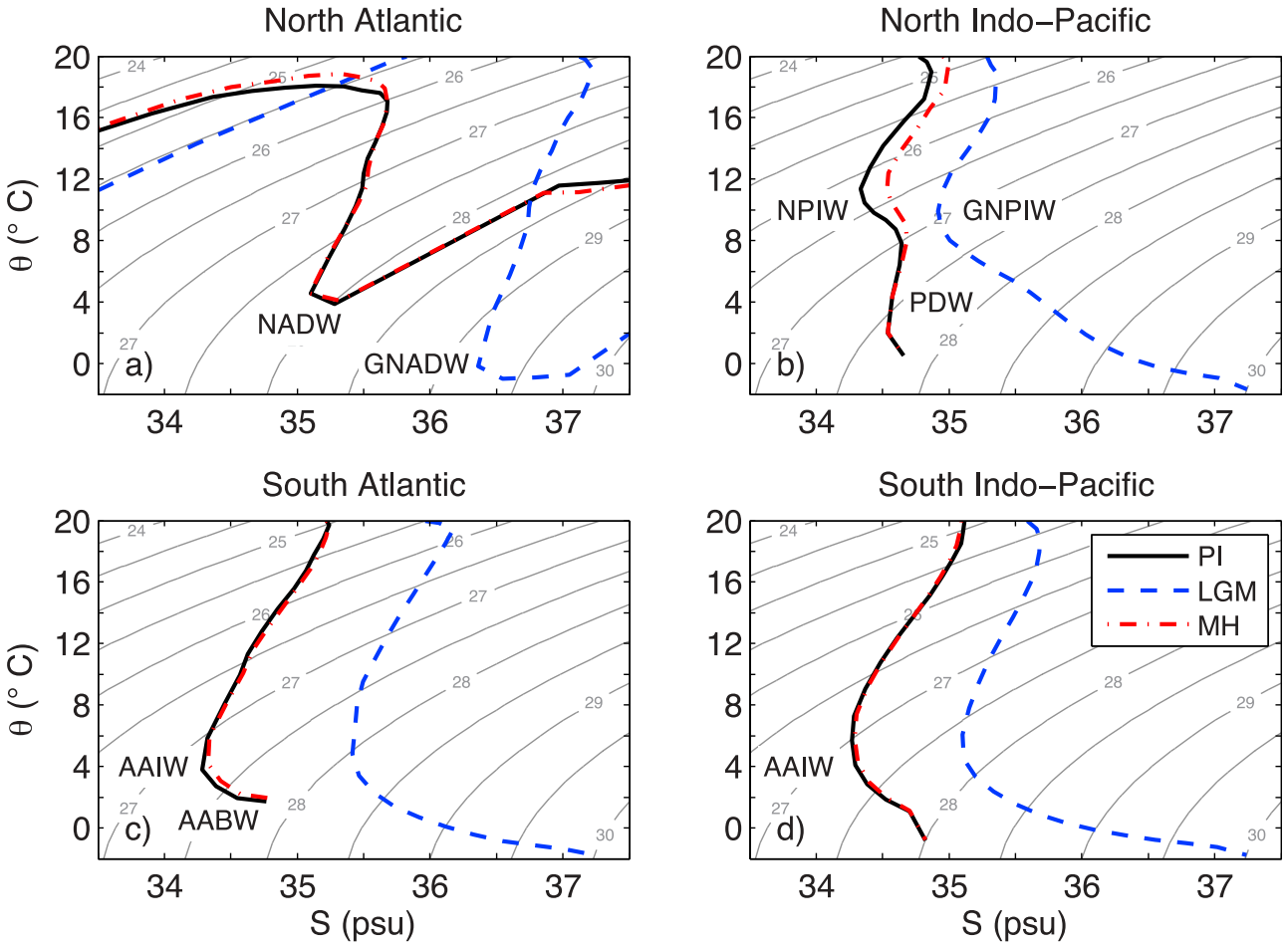

Figure 5. Mean potential temperature versus salinity (θ/S) diagrams for full-depth profiles averaged for pre-industrial (PI, black), mid-Holocene (MH, red) and LGM (blue) simulations for (a) North Atlantic, (b) North Pacific, (c) South Atlantic, and (d) South Indo-Pacific. Basin averages are defined between 15° and 60° of latitude. Isopycnals (σ_θ, kg/m^3) are also shown. The position of the main water masses are included: Antarctic Intermediate Water (AAIW); Antarctic Bottom Water (AABW); North Atlantic Deep Water (NADW); North Pacific Intermediate Water (NPIW); Pacific Deep Water (PDW).

the annual maximum mixed layer depth *H*. The mixed layer depth is calculated following the criterion of *Large et al.* [1997], and *H* is the maximum winter time mixed layer depth, averaged over the last 20 years of model integration for each run. Density at the winter mixed layer is obtained from the averaged temperature and salinity fields, and interpolated to the depth *H*. The summations over the density intervals defined in (1) are divided into $\Delta\sigma_\theta$ = 0.2 kg/m^3 increments, and includes the regions comprised from the equator to 60° meridionally in each hemisphere.

[27] Between 60°S and 60°N, the maximum H is found around the Labrador sea, reaching approximately 540 m in PI and MH, and over 1000 m in the LGM (not shown). Also in the LGM, the maximum H in the North Atlantic reaches further south (≈40°N), which agrees with the southward migration of the zero wind stress curl in that period (Figure 1), and with results from previous modeling studies [e.g., *Rahmstorf*, 2002; *Ganopolski et al.*, 1998].

[28] In the considered regions of the Southern Hemisphere, the deepest mixed layer depths are located in the formation zones of the SAMW and AAIW, ranging from 100 m to 400 m. Changes between PI and MH are small, with differences of H generally below 10 m. Indeed, according to *Liu et al.* [2003], the wind stress changes have little impact on the permanent thermocline in the mid-Holocene. In the LGM, increased wind stress and wind stress curl in the Southern Ocean cause a broad thermocline deepening of 20 to 80 m there, since more water is downwelled from the mixed layer. No shift in the zero wind stress curl line occurs among the climatic periods in the Southern ocean (Figure 1), and therefore no latitudinal migration of the deepest mixed layer depth and of the position of the Subtropical Front (STF) [*Stramma and Peterson*, 1990] is observed. It should be noted that some previous studies [e.g., *Bard and Rickaby*, 2009; *Dickson et al.*, 2009; *Vázquez Riveiros et al.*, 2010] suggest a northward migration of the South Atlantic STF for cooler stadials. Others suggest a southward migration of the STF [e.g., *Paul and Schäfer-Neth*, 2003] instead.

[29] Figure 6 shows the transport of subducted waters for 25.0 < σ_θ < 30.0 kg/m^3, for each basin (divided in north and south sub-basins) and each climatic period. At lower densities σ_θ < 26.0 kg/m^3, the subtropical waters, which are part

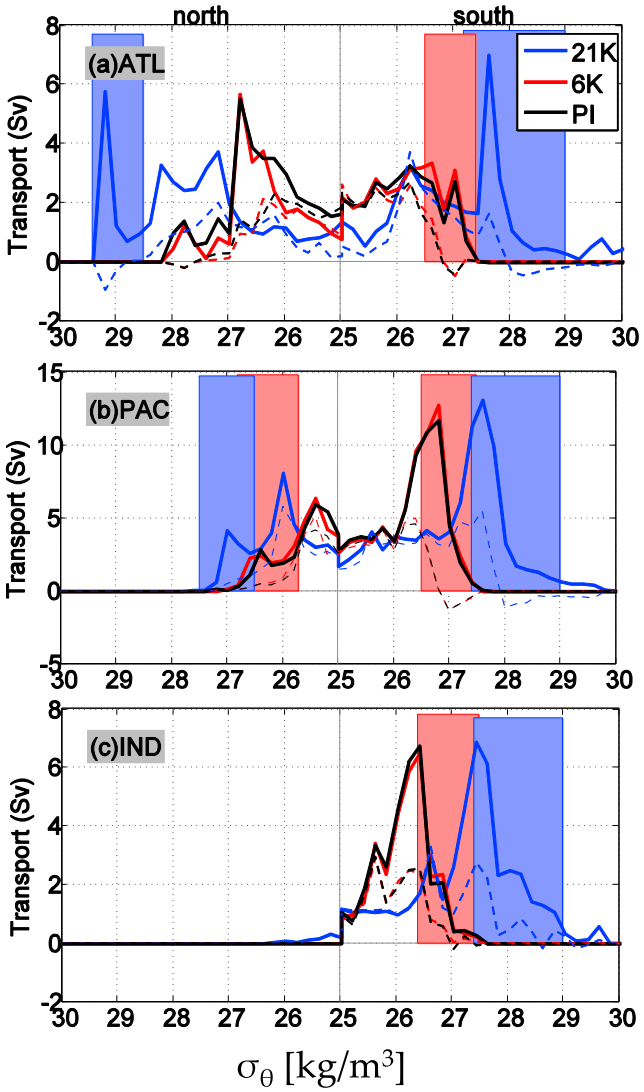

Figure 6. Transport (Sv) of subducted waters as a function of potential density σ_θ (kg m^{-3}) for the (a) Atlantic, (b) Pacific, and (c) Indian Oceans on each climatic period (black curve = PI; red curve = MH and blue curve = LGM). The vertical entrainment component of the subduction is plotted as dashed lines. The potential density range of the intermediate and the densest mode waters are shaded with the period respective color. Note that the black and red shaded areas are overlapped, since the PI and MH share similar subduction regions.

of the shallow subtropical-cells. At this range, subduction is highly driven by the vertical entrainment term (dashed lines in Figure 6). MH and PI have similar formation rates in the Southern Hemisphere in all ocean basins. *Goes et al.* [2008] also show negligible changes in subduction transports for the densities between $25.0 < \sigma_\theta < 25.8$ kg/m^3 between the 20th and 21st century. In the Northern hemisphere, changes between these two periods may be associated with changes in the wind stress curl, since the ITCZ shifts northward in the MH simulation [see *Braconnot et al.*, 2007a]. In the LGM, there is a decrease in the subduction rates in all densities in subtropical areas in the order of 2 Sv, especially in the Atlantic (Figure 6a). This is more consistent with the shrinkage of these lower density outcropping regions, since there is a systematic increase of surface density during the LGM [*Billups and Schrag*, 2000]. The region located within the $26 < \sigma_\theta < 26.9$ kg/m^3 range is largely associated with the formation region for the mode waters in the PI and MH. In the Southern Hemisphere, the SAMW formation is strongly tied to the formation of the AAIW. In the North Atlantic, mode waters have a strong formation rate, and the subduction peaks in that region are associated with formation of the subtropical mode water (STMW) and the denser subpolar mode water (SPMW) and Labrador Seawater [*Speer and Tziperman*, 1992]. In the North Pacific (Figure 6b), which is less dense, this σ_θ range is associated with formation of the NPIW [*Wong et al.*, 1999]. In the LGM, these formation regions are generally shifted to higher densities. The AAIW formation regions in the Southern Hemisphere ($26.9 < \sigma_\theta < 27.4$) show strong formation in the Indian and South Pacific basins, with a less extent in the South Atlantic basin. Indeed previous studies show that half of the AAIW formation occurs in the South Pacific [*Downes et al.*, 2010; *Karstensen and Quadfasel*, 2002].

[30] In the LGM, a strong peak is observed in the North Atlantic associated with the glacial AAIW water mass at $\sigma_\theta > 28.5$ kg/m^3, which is observed as a salinity minimum in the θ-S diagram (Figure 5b). This peak indicates vigorous water mass formation at this density class, at the expense of a deeper NADW formation in the Nordic Seas [e.g., *Curry and Oppo*, 2005; *Oppo and Fairbanks*, 1987]. The AAIW ventilation is restricted to the lower depths as seen in the section profile of Figures 3 and 4.

[31] The sum of subducted waters of SAMW and AAIW classes (Table 1), taking into account the different density ranges between the LGM and PI/MH, shows that there is a 2 Sv (20%) increase of subduction of intermediate waters in the South Atlantic for the MH, and 2 Sv (about 40%) decrease in the North Atlantic, when comparing to PI. An

Table 1. Transport (Sv) of Subducted Waters (Sub) Showing the σ_θ Range (kg m^{-3}) of the Intermediate/Mode Waters for Each Basin and Time Period

Simulation		Atlantic		Pacific		
		South	North	South	North	Indian South
PI	Sub	10.4	5.8	29.4	10.2	12.0
	σ_θ	26.5–27.4	27.4–28.2	26.5–27.5	25.7–26.8	26.4–27.5
MH	Sub	12.3	3.8	31.1	12.1	12.2
	σ_θ	26.5–27.4	27.4–28.2	26.5–27.5	25.7–26.8	26.4–27.5
LGM	Sub	16.2	8.6	43.4	10.5	24.3
	σ_θ	27.2–29.0	28.5–29.4	27.4–29.0	26.5–27.5	27.4–29.0

increase of the same magnitude is seen in the Pacific MH AAIW/SAMW formation of about 2 Sv in both northern and southern basins. In the Indian ocean negligible variability is seen in the SAMW/AAIW formation within the σ_θ = 26.4 – 27.5 kg/m^3 range, with 12.0 Sv for the PI and 12.2 Sv for the MH. The overall characteristic in CCSM3 during the LGM is a shift to higher densities during for all basins of about $\Delta\sigma_\theta$ = 1 – 1.3 kg/m^3. This is similar but with opposite sign of results from *Goes et al.* [2008] for a warmer climate. Also, except for the North Pacific, which show the same rate of NPIW formation of about 10 Sv, there is a general increase from 50% up to 100% of AAIW/SAMW formation in the LGM. The increased subduction in the North Atlantic, South Pacific and Indian basins at intermediate waters are able to replace the lack of deep water formation in those regions, and the low difference in the Atlantic meridional overturning circulation strength [see *Otto-Bliesner et al.*, 2006] confirms this result.

4. Discussion and Conclusions

[32] In the LGM, the main changes observed in the water mass formation are consistent with an intensification of the Southern Hemisphere overturning due to enhanced AABW formation. In addition, there is a 0.2–0.4 dyne/cm^2 increase in the SHZW occurs during the LGM relative to the PI.

[33] The formation and circulation of the AAIW is an important component of the upper branch of the meridional overturning circulation that is associated with the transport of heat and salt within the Southern Hemisphere subtropical gyre [*Schmitz*, 1996; *Sloyan and Rintoul*, 2001; *Talley*, 2003]. The AABW mostly forms in the Ross and Weddell Seas, spreading below NADW, and is associated with the lower branch of the MOC. Its formation is due to, among other things, a combination of sea-ice /ice-shelf melt and brine rejection. Therefore sea-ice changes in the Southern Ocean have a significant role in the modulation of changes in the oceans meridional overturning [*Goosse and Fichefet*, 1999; *Shin et al.*, 2003a].

[34] With the increased sea-ice formation and expansion at the LGM, there is an associated increase in the surface density flux off Antarctica in the Southern Oceans [*Shin et al.*, 2003a, 2003b; *Clauzet et al.*, 2007] causing deep circulation changes (i.e. enhanced AABW). As discussed by *Duplessy et al.* [1988] and *Liu et al.* [2003], paleoclimate records also suggest a shallower and weaker NADW circulation and an enhanced AABW intrusion into the North Atlantic at LGM accompanied by intensification of westerly winds and AAIW production. In fact, *McKay et al.* [2012] discuss, in the context of the late Pliocene cooling, how the intensification of Southern Hemisphere westerly winds are associated with a more vigorous ocean circulation and have been linked to increased production of AAIW at the LGM [*Muratli et al.*, 2009].

[35] Stronger SHZW is associated with enhanced northward Ekman transport which intensifies the AAIW. Previous work shows through several numerical experiments in an ocean general circulation model, that the production of AAIW is dependent on the strength of the Southern Hemisphere winds *Ribbe* [2001]. AAIW changes in ventilation have been associated with Ekman heat and freshwater transport changes caused by wind stress variability in the Southern Ocean [e.g., *Rintoul and England*, 2002; *Sallee et al.*, 2006; *Naveira Garabato et al.*, 2009].

[36] Many studies propose that the SHZW may move equatorward and perhaps weaken during glacial periods [e.g., *Toggweiler et al.*, 2006; *Bard and Rickaby*, 2009; *Dickson et al.*, 2009; *Vázquez Riveiros et al.*, 2010], both of which would reduce the northward export of Antarctic surface waters and the resulting upwelling of relatively salty deep water. An increase in the Southern Ocean upwelling during Northern Hemisphere cold intervals is consistent with several paleodata studies [e.g., *Anderson et al.*, 2009; *Skinner et al.*, 2010; *Spero and Lea*, 2002] synthesized by *Denton et al.* [2010].

[37] They suggest that climate-related shifts in the mean position of the Southern Hemisphere westerlies can be inferred from different sources of paleo-proxy data. Recent modeling results point to a link between Northern Hemisphere cooling and SHZW strengthening via a shift in the Intertropical Convergence Zone and the resulting effects on the Hadley circulation [*Lee et al.*, 2011]. Also, recent analysis of benthic foraminiferal Cd/Ca by *Makou et al.* [2010] suggest, much in agreement with the results shown in Figure 3, that the AAIW was unique to the glacial South Atlantic and that it formed differently than today.

[38] During the MH, the fresher North Atlantic shows reduced subduction in intermediate levels by 2 Sv, but increased AAIW formation by 2 Sv. In the Pacific, there is an increase of subduction in the MH for both AAIW and NPIW of 2.7 Sv, but mostly due to enhanced AAIW (2 Sv). In the LGM, both AAIW and GNAIW increase (4.2 and 5.3 Sv, respectively), meaning that both southern and northern intermediate waters contribute to replacing the lack of NADW in the LGM.

[39] In CCSM3, the increase of AAIW formation in the South Pacific and Indian Oceans does not represent increased ventilation in deep levels, since the AABW and PDW are much denser, presumably due to excess ice formation in the CCSM, and the deep ocean is more stagnant (as discussed in *Shin et al.* [2003a] and *Liu et al.* [2005]).

[40] Less upwelling of old waters would increase the carbon concentration of the deep ocean. This is consistent with *Skinner et al.* [2010] who found much older deep water circulation around Antarctica during the last glacial period. This relatively coarse resolution version of the CCSM3 can not simulate eddies, which are parameterized by the Gent and McWilliams diffusion. Increased mixing by eddies in response to strengthened winds in the polar regions could counteract the increased Ekman transport [*Meredith and Hogg*, 2006], and therefore reduce the wind-driven response during the LGM.

[41] **Acknowledgments.** This work was supported in part by grants from FAPESP, CAPES, CNPq-300223/93-5 and CNPq-MCT-INCT-Criosfera. Marlos Goes carried out this research under the auspices of the Cooperative Institute for Marine and Atmospheric Studies (CIMAS), a cooperative institute of the University of Miami and the National Oceanic and Atmospheric Administration, cooperative agreement NA17RJ1226.

References

Adkins, J., K. McIntyre, and D. Schrag (2002), The salinity, temperature, and δ^{18}O of the glacial deep ocean, *Science*, *298*(5599), 1769–1773.

Anderson, R., S. Ali, L. Bradtmiller, S. Nielsen, M. Fleisher, B. Anderson, and L. Burckle (2009), Wind-driven upwelling in the southern ocean and

the deglacial rise in atmospheric CO_2, *Science*, *323*(5920), 1443–1448, doi:10.1126/science.1167441.
Bard, E., and R. Rickaby (2009), Migration of the subtropical front as a modulator of glacial climate, *Nature*, *460*(7253), 380–383.
Billups, K., and D. P. Schrag (2000), Surface ocean density gradients during the Last Glacial Maximum, *Paleoceanography*, *15*, 110–123.
Braconnot, P., et al. (2007a), Results of PMIP2 coupled simulations of the mid-Holocene and last glacial maximum – Part 1: Experiments and large-scale features, *Clim. Past*, *3*, 261–277.
Braconnot, P., et al. (2007b), Results of PMIP2 coupled simulations of the mid-Holocene and last glacial maximum – Part 2: Feedbacks with enphasis on the location of the itcz and mid- and high latitudes heat budget, *Clim. Past*, *3*, 279–296.
Briegleb, B., C. Bitz, E. Hunke, W. Lipscomb, M. Holland, J. Schramm, and R. Moritz (2004), Scientific description of the sea ice component in the community climate system model, version three, *NCAR Tech. Note NCAR/TN-463+ STR*, NCAR, Boulder, Colo.
Clauzet, G., I. Wainer, A. Lazar, E. Brady, and B. Otto-Bliesner (2007), A numerical study of the south Atlantic circulation at the last glacial maximum, *Palaeogeogr. Palaeoclimatol. Palaeoecol.*, *253*(3–4), 509–528.
Clauzet, G., I. Wainer, and M. Bicego (2008), Validating NCAR-CCSM last glacial maximum sea surface temperature in the tropical and south Atlantic with proxy-data, *Palaeogeogr. Palaeoclimatol. Palaeoecol.*, *267*(3–4), 153–160.
Cléroux, C., P. deMenocal, and T. Guilderson (2011), Deglacial radiocarbon history of tropical Atlantic thermocline waters: Absence of CO_2 reservoir purging signal, *Quat. Sci. Rev.*, *30*, 1875–1882.
Collins, W., et al. (2006), The formulation and atmospheric simulation of the community atmosphere model: CAM3, *J. Clim.*, *19*(11), 2144–2161.
Curry, W. B., and D. W. Oppo (2005), Glacial water mass geometry and the distribution of $\delta^{13}C$ of ΣCO_2 in the western Atlantic Ocean, *Paleoceanography*, *20*, PA1017, doi:10.1029/2004PA001021.
Cushman-Roisin, B. (1987), Subduction, in *Dynamics of the Oceanic Surface Mixed Layer*, pp. 181–196, Hawaii Inst. of Geophys., Honolulu.
Dällenbach, A., T. Blunier, J. Flückiger, B. Stauffer, J. Chappellaz, and D. Raynaud (2000), Changes in the atmospheric CH_4 gradient between Greenland and Antarctica during the Last Glacial and the transition to the Holocene, *Geophys. Res. Lett.*, *27*, 1005–1008.
Denton, G., R. Anderson, J. Toggweiler, R. Edwards, J. Schaefer, and A. Putnam (2010), The last glacial termination, *Science*, *328*(5986), 1652–1656.
Dickinson, R., K. Oleson, G. Bonan, F. Hoffman, P. Thornton, M. Vertenstein, Z. Yang, and X. Zeng (2006), The community land model and its climate statistics as a component of the community climate system model, *J. Clim.*, *19*(11), 2302–2324.
Dickson, A., C. Beer, C. Dempsey, M. Maslin, J. Bendle, E. McClymont, and R. Pancost (2009), Oceanic forcing of the marine isotope stage 11 interglacial, *Nat. Geosci.*, *2*(6), 428–433.
Downes, S. M., N. L. Bindoff, and S. R. Rintoul (2010), Changes in the subduction of Southern Ocean water masses at the end of the twenty-first century in eight IPCC models, *J. Clim.*, *23*, 6526–6541, doi:10.1175/2010JCLI3620.1.
Drijfhout, S. S., J. Donners, and W. P. M. de Ruijter (2005), The origin of intermediate and subpolar mode waters crossing the Atlantic equator in OCCAM, *Geophys. Res. Lett.*, *32*, L06602, doi:10.1029/2004GL021851.
Duplessy, J., N. Shackleton, R. Fairbanks, L. Labeyrie, D. Oppo, and N. Kallel (1988), Deepwater source variations during the last climatic cycle and their impact on the global deepwater circulation, *Paleoceanography*, *3*(3), 343–360.
Fischer, H., et al. (2010), The role of southern ocean processes in orbital and millennial CO_2 variations-a synthesis, *Quat. Sci. Rev.*, *29*(1–2), 193–205.
Flückiger, J., A. Dällenbach, T. Blunier, B. Stauffer, T. Stocker, D. Raynaud, and J. Barnola (1999), Variations in atmospheric N_2O concentration during abrupt climatic changes, *Science*, *285*(5425), 227–230.
Ganopolski, A., S. Rahmstorf, V. Petoukhov, and M. Claussen (1998), Simulation of modern and glacial climates with a coupled global model of intermediate complexity, *Nature*, *391*, 351–356.
Gent, P., F. Bryan, G. Danabasoglu, K. Lindsay, D. Tsumune, M. Hecht, and S. Doney (2006), Ocean chlorofluorocarbon and heat uptake during the twentieth century in the CCSM3, *J. Clim.*, *19*(11), 2366–2381.
Goes, M., I. Wainer, P. R. Gent, and F. O. Bryan (2008), Changes in subduction in the South Atlantic Ocean during the 21st century in the CCSM3, *Geophys. Res. Lett.*, *35*, L06701, doi:10.1029/2007GL032762.
Goosse, H., and T. Fichefet (1999), Importance of ice-ocean interactions for the global ocean circulation: A model study, *J. Geophys. Res.*, *104*(C10), 23,337–23,355.
Herguera, J., T. Herbert, M. Kashgarian, and C. Charles (2010), Intermediate and deep water mass distribution in the Pacific during the last glacial maximum inferred from oxygen and carbon stable isotopes, *Quat. Sci. Rev.*, *29*(9), 1228–1245.
Joyce, T., J. Luyten, A. Kubryakov, F. Bahr, and J. Pallant (1998), Meso-to large-scale structure of subducting water in the subtropical gyre of the eastern North Atlantic ocean, *J. Phys. Oceanogr.*, *28*(1), 40–61.
Karstensen, J., and D. Quadfasel (2002), Formation of southern hemisphere thermocline waters: Water mass conversion and subduction, *J. Phys. Oceanogr.*, *32*(11), 3020–3038.
Large, W. G., G. Danabasoglu, S. C. Doney, and J. C. McWilliams (1997), Sensitivity to surface forcing and boundary layer mixing in a global ocean model: Annual-mean climatology, *J. Phys. Oceanogr.*, *27*, 2418–2447.
Lee, S.-Y., J. C. H. Chiang, K. Matsumoto, and K. S. Tokos (2011), Southern ocean wind response to North Atlantic cooling and the rise in atmospheric CO_2: Modeling perspective and paleoceanographic implications, *Paleoceanography*, *26*, PA1214, doi:10.1029/2010PA002004.
Liu, Z. (2006), Glacial thermohaline circulation and climate: Forcing from the north or south?, *Adv. Atmos. Sci.*, *23*(2), 199–206.
Liu, Z., I. Kutzbach, and L. Wu (2000), Modelling climate shift of El Nino variability in the holocene, *Geophys. Res. Lett.*, *27*(15), 2265–2268.
Liu, Z., E. Brady, and J. Lynch-Stieglitz (2003), Global ocean response to orbital forcing in the Holocene, *Paleoceanography*, *18*(2), 1041, doi:10.1029/2002PA000819.
Liu, Z., S.-I. Shin, R. S. Webb, W. Lewis, and B. L. Otto-Bliesner (2005), Atmospheric CO_2 forcing on glacial thermohaline circulation and climate, *Geophys. Res. Lett.*, *32*, L02706, doi:10.1029/2004GL021929.
Makou, M. C., D. W. Oppo, and W. B. Curry (2010), South Atlantic intermediate water mass geometry for the last glacial maximum from foraminiferal Cd/Ca, *Paleoceanography*, *25*, PA4101, doi:10.1029/2010PA001962.
Marchitto, T. M., and W. S. Broecker (2006), Deep water mass geometry in the glacial Atlantic Ocean: A review of constraints from the paleonutrient proxy Cd/Ca, *Geochem. Geophys. Geosyst.*, *7*, Q12003, doi:10.1029/2006GC001323.
Matsumoto, K., T. Oba, J. Lynch-Stieglitz, and H. Yamamoto (2002), Interior hydrography and circulation of the glacial Pacific ocean, *Quat. Sci. Rev.*, *21*, 1693–1704.
McCartney, M. S. (1977), Subantarctic Mode Water, in *A Voyage of Discovery*, edited by M. Angel, pp. 103–119, Pergamon, Oxford, U. K.
McKay, R., et al. (2012), Antarctic and Southern Ocean influences on Late Pliocene global cooling, *Proc. Natl. Acad. Sci. U. S. A.*, *109*, 6423–6428.
McNeil, B., R. Matear, R. Key, J. Bullister, and J. Sarmiento (2003), Anthropogenic CO_2 uptake by the ocean based on the global chlorofluorocarbon data set, *Science*, *299*(5604), 235–239.
Meredith, M. P., and A. M. Hogg (2006), Circumpolar response of southern ocean eddy activity to a change in the southern annular mode, *Geophys. Res. Lett.*, *33*, L16608, doi:10.1029/2006GL026499.
Monnin, E., A. Indermühle, A. Dällenbach, J. Flückiger, B. Stauffer, T. Stocker, D. Raynaud, and J. Barnola (2001), Atmospheric CO_2 concentrations over the last glacial termination, *Science*, *291*(5501), 112–114.
Muratli, J., Z. Chase, A. Mix, and J. McManus (2009), Increased glacial-age ventilation of the chilean margin by antarctic intermediate water, *Nat. Geosci.*, *3*, 23–26.
Naveira Garabato, A., L. Jullion, D. Stevens, K. Heywood, and B. King (2009), Variability of subantarctic mode water and antarctic intermediate water in the Drake passage during the late-twentieth and early-twenty-first centuries, *J. Clim.*, *22*(13), 3661–3688.
Oppo, D., and R. Fairbanks (1987), Variability in the deep and intermediate water circulation of the Atlantic ocean during the past 25,000 years: Northern Hemisphere modulation of the Southern Ocean, *Earth Planet. Sci. Lett.*, *86*(1), 1–15.
Otto-Bliesner, B., E. Brady, G. Clauzet, R. Tomas, S. Levis, and Z. Kothavala (2006), Last glacial maximum and holocene climate in CCSM3, *J. Clim.*, *19*(11), 2526–2544.
Otto-Bliesner, B. L., C. D. Hewitt, T. M. Marchitto, E. Brady, A. Abe-Ouchi, M. Crucifix, S. Murakami, and S. L. Weber (2007), Last Glacial Maximum ocean thermohaline circulation: PMIP2 model intercomparisons and data constraints, *Geophys. Res. Lett.*, *34*, L12706, doi:10.1029/2007GL029475.
Otto-Bliesner, B., et al. (2009), A comparison of PMIP2 model simulations and the margo proxy reconstruction for tropical sea surface temperatures at last glacial maximum, *Clim. Dyn.*, *32*(6), 799–815.
Pahnke, K., and R. Zahn (2005), Southern hemisphere water mass conversion linked with North Atlantic climate variability, *Science*, *307*(5716), 1741–1746.
Pahnke, K., S. Goldstein, and S. Hemming (2008), Abrupt changes in antarctic intermediate water circulation over the past 25,000 years, *Nat. Geosci.*, *1*(12), 870–874.

Paul, A., and C. Schäfer-Neth (2003), Modeling the water masses of the Atlantic Ocean at the Last Glacial Maximum, *Paleoceanography*, *18*(3), 1058, doi:10.1029/2002PA000783.

Peltier, W. R. (2004), Global glacial isostasy and the surface of the ice-age Earth: The ICE-5G (VM2) model and GRACE, *Annu. Rev. Earth Planet. Sci.*, *32*, 111–149.

Rahmstorf, S. (2002), Ocean circulation and climate during the past 120,000 years, *Nature*, *419*, 207–214.

Ribbe, J. (2001), Intermediate water mass production controlled by Southern Hemisphere winds, *Geophys. Res. Lett.*, *28*(3), 535–538.

Rintoul, S., and M. England (2002), Ekman transport dominates local air-sea fluxes in driving variability of subantarctic mode water, *J. Phys. Oceanogr.*, *32*(5), 1308–1321.

Sabine, C., and T. Tanhua (2010), Estimation of anthropogenic CO_2 inventories in the ocean, *Annu. Rev. Mar. Sci.*, *2*, 175–198.

Sabine, C., et al. (2004), The oceanic sink for anthropogenic CO_2, *Science*, *305*(5682), 367–371.

Sallee, J., N. Wienders, K. Speer, and R. Morrow (2006), Formation of subantarctic mode water in the southeastern Indian ocean, *Ocean Dyn.*, *56*(5), 525–542.

Schmitz, W. J. (1996), On the world ocean circulation, vol. 2, The Pacific and Indian Oceans: A global update, *Tech. Rep. WHOI-96-08*, Woods Hole Oceanogr. Inst., Woods Hole, Mass.

Shin, S., Z. Liu, B. Otto-Bliesner, E. Brady, J. Kutzbach, and S. Harrison (2003a), A simulation of the Last Glacial Maximum climate using the NCAR-CCSM, *Clim. Dyn.*, *20*(2), 127–151.

Shin, S., Z. Liu, B. Otto-Bliesner, J. Kutzbach, and S. Vavrus (2003b), Southern ocean sea-ice control of the glacial North Atlantic thermohaline circulation, *Geophys. Res. Lett.*, *30*(2), 1096, doi:10.1029/2002GL015513.

Skinner, L., S. Fallon, C. Waelbroeck, E. Michel, and S. Barker (2010), Ventilation of the deep Southern Ocean and deglacial CO_2 rise, *Science*, *328*(5982), 1147–1151, doi:10.1126/science.1183627.

Sloyan, B., and S. Rintoul (2001), Circulation, renewal, and modification of antarctic mode and intermediate water, *J. Phys. Oceanogr.*, *31*(4), 1005–1030.

Sloyan, B. M., and I. V. Kamenkovich (2007), Simulation of subantarctic mode and antarctic intermediate waters in climate models, *J. Clim.*, *20*(20), 5061–5080, doi:10.1175/JCLI4295.1.

Søørensen, J. V. T., J. Ribbe, and G. Shaffer (2001), Antarctic intermediate water mass formation in ocean general circulation models, *J. Phys. Oceanogr.*, *31*, 3295–3311, doi:10.1175/1520-0485(2001)031.

Speer, K., and E. Tziperman (1992), Rates of water mass formation in the North Atlantic, *J. Phys. Oceanogr.*, *22*, 93–104.

Spero, H., and D. Lea (2002), The cause of carbon isotope minimum events on glacial terminations, *Science*, *296*(5567), 522–525.

Stommel, H. (1979), Determination of water mass properties of water pumped down from the ekman layer to the geostrophic flow below, *Proc. Natl. Acad. Sci. U. S. A.*, *76*, 3051–3055.

Stramma, L., and R. Peterson (1990), The South Atlantic Current, *J. Phys. Oceanogr.*, *20*(6), 846–859.

Taft, B. A. (1963), Distribution of salinity and dissolved oxygen on surfaces of uniform potential specific volume in the south Atlantic, south Pacific and Indian oceans, *J. Mar. Res.*, *21*, 129–146.

Talley, L. (1993), Distribution and formation of North Pacific intermediate water, *J. Phys. Oceanogr.*, *23*, 517–517.

Talley, L. (1996), Antarctic Intermediate Water in the South Atlantic, in *The South Atlantic: Present and Past Circulation*, edited by G. Weferet et al., pp. 219–238, Springer, Berlin.

Talley, L. D. (1999), Some aspects of ocean heat transport by the shallow, intermediate and deep overturning circulations, in *Mechanisms of Global Climate Change at Millennial Time Scales*, *Geophys. Monogr. Ser.*, vol. 112, edited by U. Clark, S. Webb, and D. Keigwin, pp. 1–22, AGU, Washington, D. C., doi:10.1029/GM112p0001.

Talley, L. D. (2003), Shallow, intermediate, and deep overturning components of the global heat budget, *J. Phys. Oceanogr.*, *33*(3), 530–560.

Toggweiler, J. (1999), Variation of atmospheric CO_2 by ventilation of the ocean's deepest water, *Paleoceanography*, *14*(5), 571–588, doi:10.1029/1999PA900033.

Toggweiler, J., J. Russell, and S. Carson (2006), Midlatitude westerlies, atmospheric CO_2, and climate change during the ice ages, *Paleoceanography*, *21*, PA2005, doi:10.1029/2005PA001154.

Vázquez Riveiros, N., C. Waelbroeck, L. Skinner, D. Roche, J. Duplessy, and E. Michel (2010), Response of South Atlantic deep waters to deglacial warming during terminations V and I, *Earth Planet. Sci. Lett.*, *298*(3–4), 323–333.

Wong, A., N. Bindoff, and J. Church (1999), Large-scale freshening of intermediate waters in the Pacific and Indian oceans, *Nature*, *400*(6743), 440–443.